Pulsed Plasma Polymerization of Thiophene

L. M. H. Groenewoud, G. H. M. Engbers, J. G. A. Terlingen, H. Wormeester,† and J. Feijen*

Department of Chemical Technology, Section Polymer Chemistry and Biomaterials and Institute for Biomedical Technology (BMTI), and Department of Applied Physics, Section Solid State Physics, University of Twente, PO Box 217, 7500 AE Enschede, The Netherlands

Received January 28, 2000. In Final Form: March 20, 2000

Highly transparent (>80%) and conductive layers (10^{-6} S/cm) were obtained by the pulsed plasma polymerization of thiophene. The influence of power, pressure, pulse time, duty cycle, and position in the reactor on the conductivity of the resulting plasma polymerized thiophene (PPT) layers was evaluated. In the used ranges, only pressure had a significant influence on the conductivity of the deposited layer. The results could be correlated to the effect of the deposition parameters on the fragmentation of the thiophene monomer. At high pressure there was less fragmentation of thiophene, resulting in a higher conductivity of the layer. It was shown that the use of a pulsed plasma as a means to minimize fragmentation is most efficient when the off time is chosen such that the reactor is replenished with new monomer during the off period.

Introduction

Materials that combine conductivity with polymeric properties such as flexibility and processability can be used in a number of applications, e.g. polymeric batteries, flexible LCDs, and antistatic coatings.[1−6] For a polymer to be conductive, a conjugated system is required. For example, polythiophene is known for its high (10^3 S/cm) and stable conductivity.[7−10] Due to the nature of the conjugated system, conductive polymers are nontransparent and intractable, which is also the case for polythiophene.[11]

Several authors have investigated the effect of the length of the conjugated sequences in polythiophene on conductivity. For instance, ten Hoeve et al. found that an oligomer with 11 thiophene units has the same conductivity as polythiophene with a higher molecular weight.[12] Garnier's group found that relatively short oligomers of thiophene show many of the properties of the polymer.[13] The carrier mobility and the conductivity increase with increasing conjugation length up to the hexamer of thiophene.

For certain applications where conductivity is necessary, the transparency is of major importance (e.g. antistatic coatings on photographic films, LCDs) and should generally be higher than 90%. By "dilution" of the conductive polymer the transparency can be increased, but usually this will also result in a decrease in conductivity. Some of the applications where transparency is needed require only a low conductivity. For instance, antistatic coatings should have a surface conductivity of 10^{-6}−10^{-11} S. Several methods are available for the dilution of polythiophene, for example, the grafting of alkyl side chains onto the conjugated backbone,[14,15] block-copolymerization[16] or blending with a transparent polymer,[17,18] and making composites by polymerization of thiophene absorbed in an insulating polymer.[19] Furthermore, very thin layers of polythiophene can be deposited by electrochemical procedures[14] and plasma polymerization.[20−26] The latter technique offers the possibility to obtain very thin, pinhole-free layers which adhere tightly to almost any substrate, without the use of solvents.[27,28] Sadhir et al. prepared plasma polymerized thiophene (PPT) layers using argon as an initiator (4 W, 0.1 mbar, coil configuration). After overnight doping with iodine, conductivities ranging from 10^{-6} to 10^{-4} S/cm were obtained. Films deposited at positions away from the high rf-flux region (i.e. away from the coil) showed a higher conductivity than films deposited

* To whom correspondence should be addressed.
† Department of Applied Physics.

(1) Ellis, J. R. In *Handbook of Conducting Polymers*; Skotheim, T. A., Ed.; Marcel Dekker Inc.: New York, 1986; Vol. 1, pp 489−500.
(2) Saunders: H. E. *Machine Design* **1992**, 161−165.
(3) Bäuerle, P. *Adv. Mater.* **1993**, *5*, 879−885.
(4) Miller, J. S. *Adv. Mater.* **1993**, *5*, 587−589.
(5) Beyer, G. *Polym. News* **1993**, *18*, 325−327.
(6) Mooney, P. J. *JOM* **1994**, *March*, 44−45.
(7) Schopf, G.; Kossmehl, G. *Adv. Polym. Sci.* **1997**, *129*.
(8) Tourillon, G. In *Handbook of Conducting Polymers*; Skotheim, T. A., Ed.; Marcel Dekker: New York, 1986; Vol. 1, pp 293−350.
(9) Leclerc, M.; Faïd, K. *Adv. Mater.* **1997**, *9*, 1087−1094.
(10) Yamamoto, T.; Sanechika, K.; Yamamoto, A. *J. Polym. Sci., Polym. Lett. Ed.* **1980**, *18*, 9−12.
(11) Feast, W. J.; Tsibouklis, J.; Pouwer, K. L.; Groenendaal, L.; Meijer, E. W. *Polymer* **1996**, *37*, 5017−5047.
(12) Tenhoeve, W.; Wynberg, H.; Havinga, E. E.; Meijer, E. W. *J. Am. Chem. Soc.* **1991**, *113*, 5887−5889.
(13) Garnier, F.; Deloffre, F.; Horowitz, G.; Hajlaoui, R. *Synth. Met.* **1993**, *57*, 4747−4754.
(14) Glenis, S.; Benz, M.; LeGoff, E.; Kanatzidis, M. G.; Groot, D. C. d.; Schindler, J. L.; Kannewurf, C. R. *Synth. Met.* **1995**, *75*, 213−221.
(15) Zotti, G.; Salmaso, R.; Gallazzi, M. C.; Marin, R. A. *Chem. Mater.* **1997**, *9*, 791−795.
(16) Yin, W.; Li, J.; Gu, T.; Wu, J. *J. Appl. Polym. Sci.* **1997**, *63*, 13−16.
(17) Laakso, J.; Osterholm, J. E.; Nyholm, P. *Synth. Met.* **1989**, *28*, C467−C471.
(18) Isotalo, H.; Ahlskog, M.; Stubb, H.; Laakso, J.; Karna, T.; Jussila, M.; Osterholm, J. E. *Synth. Met.* **1993**, *57*, 3581−3586.
(19) Meador, M. A. B.; Hardy-Green, D.; Auping, J. V.; Gaier, J. R.; Ferrara, L. A.; Papadopoulos, D. S.; Smith, J. W.; Keller, D. J. *J. Appl. Polym. Sci.* **1997**, *63*, 821−834.
(20) Tanaka, K.; Yoshizawa, K.; Takeuchi, T.; Yamabe, T.; Yamauchi, J. *Synth. Met.* **1990**, *38*, 107−116.
(21) Sadhir, R. K.; K. F. Schoch, J. *Polym. Prepr.* **1992**, *33*, 412−413.
(22) Sadhir, R.; K. F. Schoch, J. *Thin Solid Films* **1993**, *223*, 154−160.
(23) Sadhir, R.; K. F. Schoch, J. *Polym. Prepr.* **1995**, *34*, 679−680.
(24) Tanaka, K.; Okazaki, S.; Inomata, T.; Kogoma, M. *Symp. Plasma Sci. Mater.* **1995**, *8*, 33−37.
(25) Giungato, P.; Ferrara, M. C.; Musio, F.; d'Agostino, R. *Plasmas Polym.* **1996**, *1*, 283−297.
(26) Kiesow, A.; Heilmann, A. *Thin Solid Films* **1999**, *344*, 338−341.
(27) Boenig, H. V. *Encyclopedia of Polymer Science and Engineering*; H. F. Mark, J. I. K., Ed., 1986; Vol. 11, pp 248−261.
(28) Yasuda, H. *Plasma polymerization*; Academic Press: Orlando, 1985.

10.1021/la000111b CCC: $19.00
Published on Web 06/22/2000

near the coil.[21−23] Tanaka et al. investigated the effect of plasma frequency (af vs rf, bell jar configuration) on the conductivity of argon-initiated PPT layers. Although Fourier transform infrared (FTIR) measurements did not indicate the presence of thiophene rings in the layers, conductivities ranging from 10^{-3} (af, 100 W) to 10^{-4} S/cm (rf, 25 W) were found after 5 h doping with iodine.[20] In situ doping was carried out by Giungato et al., using a mixture of argon, thiophene and iodine (5 W, 0.67 mbar, two internal electrodes). On the basis of FTIR measurements it was concluded that, although fragmentation had taken place during deposition, the thiophene ring was preserved to some extent in the PPT layer. A conductivity of 10^{-5} S/cm was obtained for the PPT layers, without additional doping.[25] Depositions at atmospheric pressure were carried out by Tanaka et al. using helium as diluent.[24] A higher conductivity was observed for PPT layers containing more conjugation.

In the studies cited above, noble gases were used as initiators to prepare PPT layers with an enhanced preservation of the monomer structure. The authors hypothesized that this improves the conductivity of the resulting PPT layer. From the literature it is known that pulsed plasma polymerization in general results in a higher retention of the monomer structure than continuous wave (CW) plasma polymerization.[29−33] Therefore, an alternative method to preserve the monomer structure in the PPT layer may be the application of a pulsed plasma. To our knowledge, no pulsed plasma polymerization of thiophene has been reported until now. Furthermore, the transparency of the PPT layers and the effect of plasma deposition parameters on the preservation of the monomer structure in the PPT layers has not been studied in detail.

In this study a pulsed plasma is used to obtain transparent and conductive PPT layers. The effect of different deposition parameters (power, pressure, pulse time (t_{on}), duty cycle [$t_{on}/(t_{on} + t_{off})$], and substrate position in the reactor) on the electrical properties of the PPT layers after iodine doping is evaluated. X-ray photoelectron spectroscopy (XPS) and FTIR are used to get insight into the relation between chemical composition/structure and the electrical properties of the PPT layers. The plasma phase is characterized using mass spectrometry (MS) and optical emission spectroscopy (OES). The transparency of the deposited PPT layers is determined with ellipsometry.

Experimental Section

Materials. Thiophene (99.5% purity) was purchased from Merck (Darmstadt, Germany). All solvents were of analytical grade purity and were also purchased from Merck. Water used was doubly deionized. All chemicals were used as received. Glass slides (∅ 2.5 cm, used for FTIR analysis) with a sputtered chromium and gold layer were obtained from the FFW division (Department of Physics and Electrical Engineering, University of Twente, The Netherlands). Glass slides (∅ 1.5 cm, used for XPS analysis) were purchased from Knittel (Braunschweig, Germany). The samples used for the conductivity measurements (glass slides with four electrodes with extensions to contact areas for the measurement leads) were supplied by the MESA Institute (University of Twente, Enschede, The Netherlands). 2,2′,5′,2″-terthiophene (T_3) was synthesized according to literature and had the characteristics reported therein (mp 92.3-93.5 °C, ^{13}C NMR ($CDCl_3$) after recrystallization from *n*-heptane: 137.1 (2,2″), 136.2 (2′,5′), 127.9 (4,4″), 124.5 (5,5″), 124.3 (3′,4′), 123.7 (3,3″) ppm).[34,35]

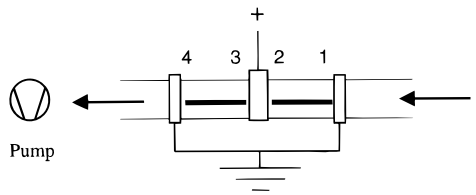

Figure 1. Schematic drawing of the plasma apparatus. The arrows indicate the direction of the gas flow. The thick lines represent the glass plates on which the samples are located. The numbers refer to the position of samples in the reactor.

Cleaning. All glassware, substrates, and tools were cleaned ultrasonically consecutively three times in toluene, hexane, acetone, water, and acetone and subsequently dried in vacuo at room temperature.

Plasma Polymerization. A schematic picture of the plasma apparatus is shown in Figure 1. In short, it consists of a tubular glass reactor (length 1.5 m, internal diameter 10 cm) with three externally placed, capacitively coupled electrodes. The powered (hot) electrode was placed at the center of the reactor. The grounded (cold) electrodes were placed at 30 cm on either side of the hot electrode. The flow of monomer vapor through the reactor was calculated from the rate of the pressure increase in the reactor (no pumping), assuming ideal gas behavior. Mass flow controllers (MKS Instruments, Andover, MA) controlled the flow of noncondensing gases. The system (without the substrates) was first cleaned by applying an air plasma (5 sccm/min, 85 W, 0.12 mbar) for 60 min. The substrates were placed on two glass plates (see Figure 1 for positions), which were placed at the center between the hot and cold electrodes, and the reactor was evacuated to base pressure ($<5 \times 10^{-4}$ mbar). The substrates were cleaned with an air plasma (5 sccm/min, 85 W, 0.12 mbar) for 5 min, after which the reactor was again evacuated to base pressure. Subsequently, monomer flow was established through the reactor, and after 2 min, pulsed plasma depositions were carried out with varying power, pressure, pulse time (t_{on}), and duty cycle [$t_{on}/(t_{on} + t_{off})$]. The total plasma "on" time was always 100 s. The pressure in the reactor was controlled by the temperature of the monomer. After deposition, the monomer flow was sustained for another 2 min and the reactor was brought to atmospheric pressure with air. The samples were stored at −18 °C.

Characterization of Plasma Phase. Mass spectrometry was carried out to analyze the gas composition at the outlet of the reactor. The spectrometer was a differentially pumped QMS 421 mass spectrometer (Blazers, Utrecht, The Netherlands). The pressure in the mass spectrometer was kept constant at 5×10^{-6} mbar using a leak valve.

OES analysis was carried out using a MCPD-1000 spectrophotometer (Otsuka, Osaka, Japan) with a slit width of 0.2 mm. The measuring probe was placed at the reactor entrance in line of sight of the plasma. Spectra were recorded from 180 to 875 nm with a step width of 2 nm.

Characterization of PPT Layers. The conductivity of the PPT layers was determined using specially designed electrodes as substrates for deposition (configuration in accordance with ASTM D257; see Figure 2A). During plasma deposition, the contact areas were covered with glass slides to locally prevent deposition. The samples were doped immediately after deposition by placing them in iodine vapor for 5 min. A current was applied through the outer electrodes and after 1 min the voltage drop was measured over the inner electrodes, using Keithley 617 electrometers (Keithley Instruments, Cleveland, OH). The volume and surface conductivities of the deposited layers were

(29) Calderon, J. G.; Timmons, R. B. *Polym. Prepr.* **1997**, *38*, 1073−1074.
(30) Mackie, N. M.; Fisher, E. R. *Polym. Prepr.* **1997**, *38*, 1059−1060.
(31) Wang, J.-H.; Chen, X.; Chen, J.-J.; Calderon, J. G.; Timmons, R. B. *Plasmas Polym.* **1997**, *2*, 245−260.
(32) Calderon, J. G.; Timmons, R. B. *Macromolecules* **1998**, *31*, 3216−3224.
(33) Han, L. M.; Timmons, R. B. *Chem. Mater.* **1998**, *10*, 1422−1429.
(34) Wynberg, H.; Metselaar, J. *Synth. Commun.* **1984**, *14*, 1−9.
(35) Carpita, A.; Rossi, R.; Veracini, C. A. *Tetrahedron* **1985**, *41*, 1919−1929.

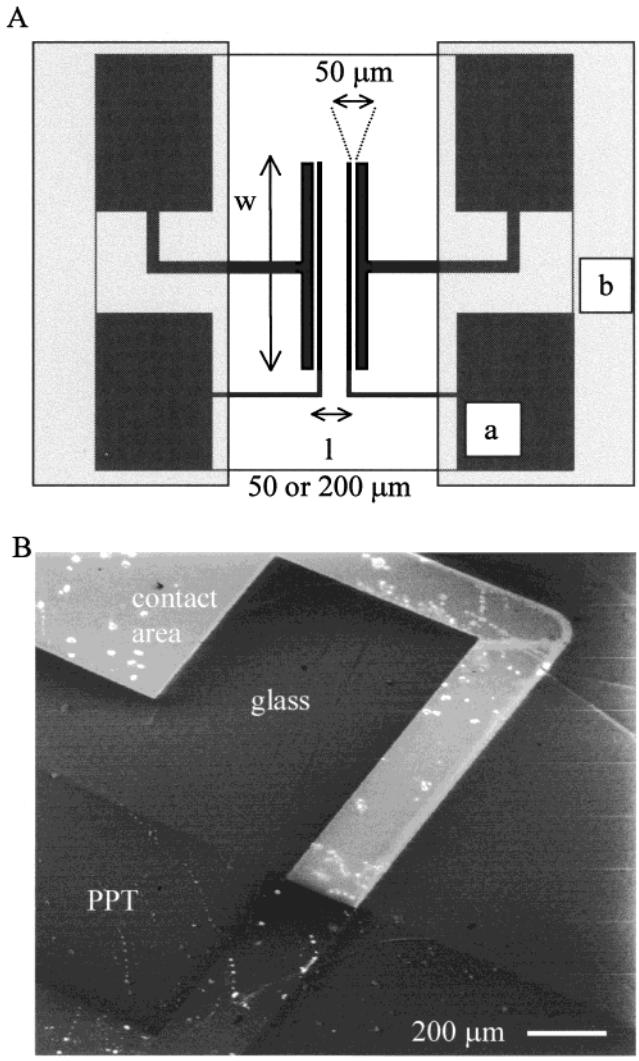

Figure 2. (A) Schematic drawing of samples with the predeposited electrodes and extensions to contact areas (a) used for the conductivity measurements. During deposition the samples are partially covered by glass slides (b). (B) SEM picture of a sample used for conductivity measurements, partly covered by a PPT layer.

calculated with the following formulas:

$$\sigma_{vol} = (I/U) \times (l/wd)\ [\mathrm{S/cm}] \quad (1)$$

$$\sigma_{surf} = (I/U) \times (l/w)\ [\mathrm{S}] \quad (2)$$

in which σ = conductivity, U = the measured voltage [V], I = the applied current [A], w = the length of the electrodes [cm], d = thickness of the PPT layer [cm], and l = the distance between electrodes [cm].

On the same samples used for the conductivity measurements the thickness of the deposited PPT layers (d) was determined with a profilometer (Dektak IIA, Sloan Technology Corporation, Santa Barbara, CA). The needle was moved over the boundary between areas of the substrate, which were covered and not covered during plasma deposition. The height difference was taken as the thickness of the deposited layer.

For FTIR analysis, PPT layers were deposited on gold-coated glass disks (∅ 2.5 cm) and spectra were recorded using a Bio-Rad FTS-60 (Cambridge, UK) in the reflectance mode. A background spectrum was recorded using a clean substrate. For the FTIR analysis of T_3, this compound was mixed into a KBr pellet, and spectra were recorded in the transmission mode.

XPS analysis of PPT layers was carried out on layers deposited on glass disks (∅ 1.5 cm) using a Kratos XSAM 800 (Manchester, UK) equipped with a Mg Kα source (1253.6 eV). The analyzer was placed perpendicular to the sample surface. The input power was 150 W (10 mA, 15 kV). The analyzed spot size was 3 mm × 6 mm. Survey scans [1100−0 eV binding energy (BE) window] were recorded with a pass energy (PE) of 100 eV and a dwell of 0.1 s. Relative peak areas for the different elements were calculated by numerical integration of the detail scans (20 eV BE window, 50 eV PE) using empirically determined sensitivity factors. After normalization, the concentrations of the various elements were obtained.

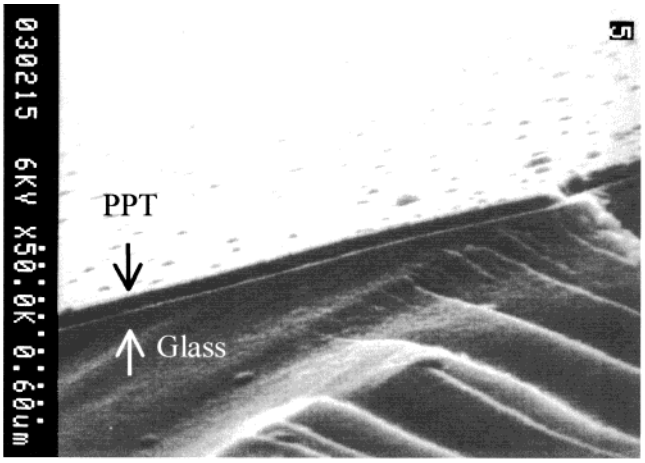

Figure 3. SEM picture of a 30 nm thick PPT layer deposited on glass. The small dots on the PPT layer are due to the gold sputtering used for sample preparation.

The transparency and the thickness of PPT layers deposited on silicon wafers were determined with ellipsometry. The instrument used was a home-built rotating polarizer type (frequency 67 Hz),[36] equipped with a 75W Xe lamp and a photomultiplier. The instrument was calibrated using the residue method. An energy scan (1.5−4.2 eV) was made recording the ellipsometric parameters (Ψ and Δ) at an angle of incidence of 70°. From these values the refractive index and optical absorption of the layers were calculated, which were used to derive the effective penetration depth of the incident light in the layer (d_{eff}). At d_{eff} two-thirds of the incident light has been absorbed. The transparency of a deposited layer can then be calculated from the intensity of the reflected light (I) and d_{eff}.

$$T = I/I_0 = \exp(-d/d_{eff}) \quad (3)$$

With T = the transparency, I = the intensity of reflected light at a certain wavelength, I_0 = the intensity of incident light at a certain wavelength, d = the thickness of the layer, and d_{eff} = the effective optical thickness.

The surface morphology of the PPT layers was studied by scanning electron microscopy (SEM) analysis using a Hitachi S-800 field emission SEM (6 kV, 20° tilt).

Results and Discussion

Plasma polymerization of thiophene resulted in homogeneous and pinhole-free PPT layers, as can be seen in Figure 3. The thickness of the PPT layers as a function of the number of pulses was determined from the ellipsometric measurements and is shown in Figure 4. The optical properties of the PPT layer were modeled with a Lorentzian absorption profile. The parameters, i.e., the PPT layer thickness and the characteristic parameters for the Lorentzian profile, were optimized in a nonlinear fit. A linear increase with the plasma "on" time is found (irrespective of the plasma "off" time), indicating that deposition only takes place during the plasma on time. Similar results were found by Uchida et al. for the plasma

(36) Wentink, D. J. *Optical reflection studies of Si and Ge (001) surfaces*; University of Twente: Enschede, 1996.

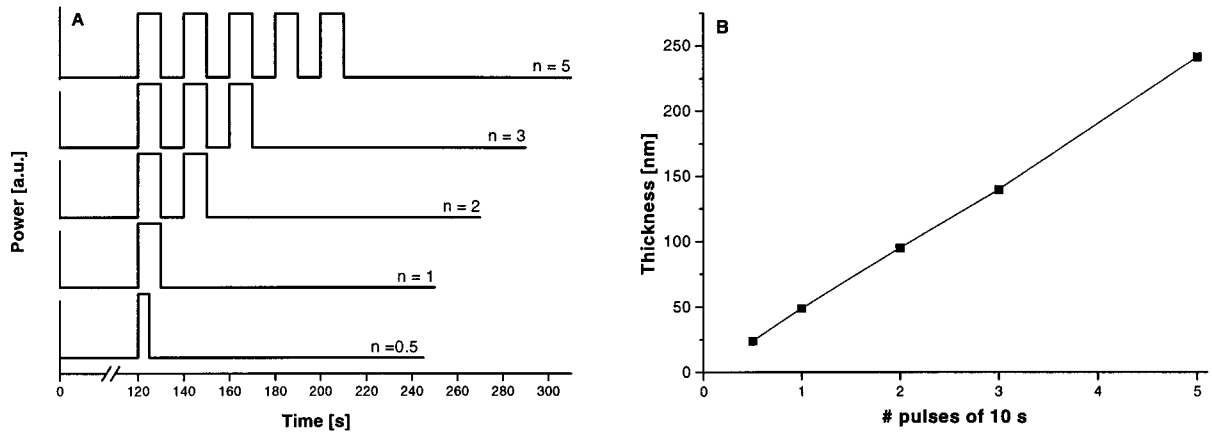

Figure 4. Thickness (as determined by ellipsometry) of PPT layers (0.06 mbar, 115 W) as a function of the number of pulses of 10 s (B). Power input as a function of time (A) for the pulsed plasma deposition of the layers used in Figure 4B. Step height is 115 W.

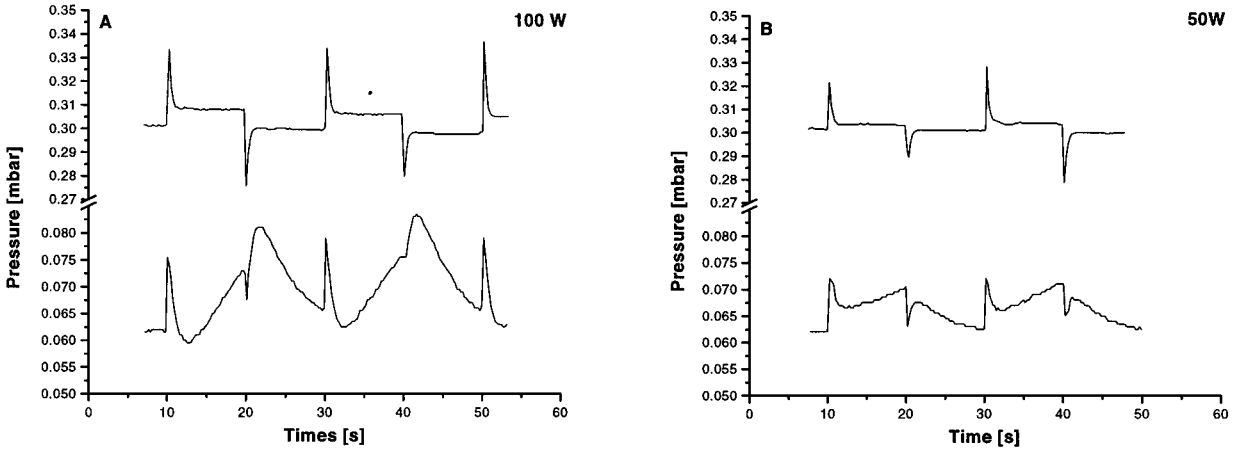

Figure 5. Course of the pressure in the reactor during plasma polymerization (10 s on, duty cycle 0.5) at different initial pressures (0.3 and 0.06 mbar) at 100 W (A) and 50 W (B). The spikes in the spectra are due to turning on/shutting off the plasma.

Table 1. Increase in the Number of Plasma Species[a] during Pulsed Plasma Deposition (10 s on, 10 s off) at Different Initial Pressures and Power Inputs

pressure (mbar)	100 W	50 W
0.06	102 (33.6%)	41.3 (13.6%)
0.3	34.0 (2.5%)	12.1 (0.8%)

[a] In μmol and between brackets in % of the initial number of species, calculated from the pressure increase during the plasma pulse (Figure 5).

polymerization of acetylene.[37,38] In Figure 5 the course of the pressure during plasma polymerization is depicted for different starting pressures and power inputs. In all cases, the pressure increases when a plasma is generated. The increase in pressure is larger at high power input and low starting pressure than at low power input and high starting pressure, respectively. Furthermore, the pressure is almost instantly constant at a high starting pressure, whereas at low starting pressure the pressure increases continuously during the plasma pulse. Table 1 gives the increase in the number of species during the plasma on time as calculated from the pressure increase during a pulse of 10 s. It was assumed that the ideal gas law holds and that the temperature does not change during deposition. Other measurements showed that for air, CF_4, and CO_2 plasmas the temperature increase in the plasma phase is less than 10 °C for pulse times <10 s.[39] From Table 1 it is clear that at high power input and low starting pressure both the relative and absolute increase in the number of species is much larger than at low power input and high starting pressure.

A balance over the reactor with respect to the number of species gives insight into the cause for the increase in pressure during the plasma on time. During plasma polymerization, plasma species are brought in by flow (monomer) and are generated by fragmentation, whereas they are removed by flow, deposition, and recombination. Assuming that the flow of species in and out of the reactor is the same at a given pressure, a pressure increase means that more species are generated by fragmentation than are removed by recombination and/or deposition ("netto" fragmentation). The deposition rate increases with increasing power input and decreasing starting pressure (data not shown). Based on the fact that oligomers of thiophene are much less volatile (for instance, T_3 only sublimates and no peaks appear in the MS), it might be assumed that there is a positive relation between recombination and deposition. The larger pressure increase at high power and low starting pressure then indicates that more fragmentation takes place at high power input and low starting pressure. Furthermore, at low pressure, netto fragmentation is taking place continuously, whereas at

(37) Uchida, T.; Senda, K.; Vinogradov, G. K.; Morita, S. *Thin Solid Films* **1996**, *281−282*, 536−538.

(38) Uchida, T.; Vinogradov, G. K.; Morita, S. *J. Electrochem. Soc.* **1997**, *144*, 1434−1439.

(39) OldeRiekerink, M. B. Private communication.

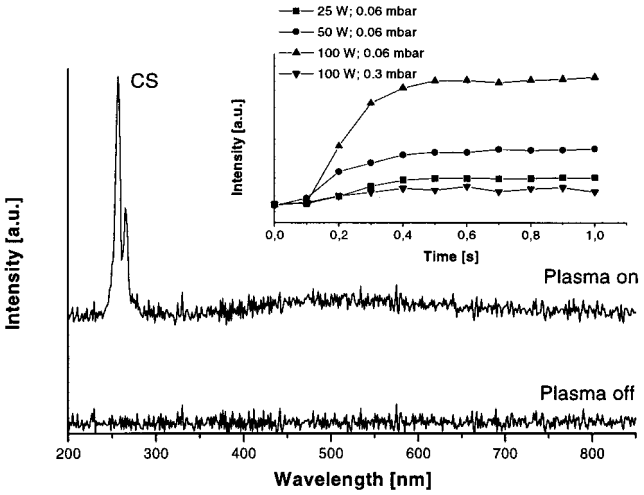

Figure 6. OES spectra of a thiophene flow (0.06 mbar) without (bottom) and with (upper, 100 W) plasma generation. The inset shows the intensity of the CS peak (256 nm) at different power inputs (at 0.06 mbar) and pressures.

high pressure an equilibrium between fragmentation and deposition/recombination is reached.

The effect of power input on the fragmentation is explained by the fact that in a rf system an increase in power input results in an increase in electron density.[40] As these electrons have sufficient energy (about 0−20 eV) to cause cleavage of covalent bonds (bond energy 3−8 eV), more electrons cause the fragmentation of more molecules. Pressure affects the plasma in several ways. First, the mean free path of plasma species will be less at higher pressure. This results in a lower average energy of the collisions (i.e. lesser degree of fragmentation). Second, in our case a higher pressure inherently results in a higher flow rate. This means that the residence time of the species in the plasma is decreased at higher pressure. The species are thus subjected to the plasma for a shorter time. Both effects result in a lesser degree of fragmentation.

Characterization of the Plasma Phase. OES and MS were used to determine the nature of the species present in the plasma phase. In the OES spectra depicted in Figure 6 two new peaks at 256 and 265 nm appear when a plasma is applied. According to literature, light of these wavelengths is emitted by the decay of excited CS species,[41] indicating that fragmentation of at least part of the thiophene molecules is taking place. As was expected on the basis of the pressure measurements, the intensity of these peaks increases with increasing power and decreasing pressure (inset of Figure 6). The course of the CS peak in time shows that after 0.5 s the CS peak intensity reaches a plateau value, irrespective of the power input. For the high starting pressure this corresponds well with the course of the pressure during the plasma pulse (Figure 5). Apparently, an equilibrium between the formation and the decay of excited CS species is reached. However, at low starting pressure an increase in pressure is still observed after 0.5 s. This means that, although netto fragmentation still occurs (Figure 5), this does not result in the formation of additional excited CS species. Furthermore, Figure 6 shows that short pulse times (<0.2 s) should be used to minimize fragmentation.

Figure 7 shows the mass spectra of a thiophene flow through the reactor with and without plasma generation.

(40) d'Agostino, R. *Plasma deposition, treatment, and etching of polymers*; Academic Press: Boston, 1990.

(41) Pearse, R. W. B.; Gaydon, A. G. *The identification of molecular spectra*, 4th ed.; Chapman and Hall: London, 1976.

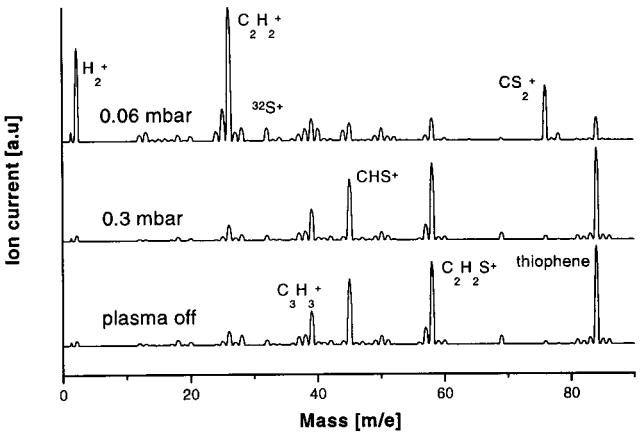

Figure 7. MS spectra of a thiophene flow without plasma generation (bottom) and with plasma generation at 0.3 mbar, 100 W (middle) and at 0.06 mbar, 100 W (top).

Table 2. Peak Assignment of Peaks Appearing (x) in the Mass Spectrum (range 0−225 *m/e*) of a Thiophene Flow with and without Plasma Generation (Figure 7)

peak (*m/e*)[a]	assignment	plasma off	plasma on
84	$C_4H_4S^+$	x	decreased
76	CS_2^+		x
58	$C_2H_2S^+$	x	decreased
45	CHS^+	x	decreased
39	$C_3H_3^+$	x	decreased
32	$^{32}S^+$		x
26	$C_2H_2^+$		x
12	C^+		x
2	H_2^+		x

[a] No peaks were observed in the range of 85−225 *m/e*.

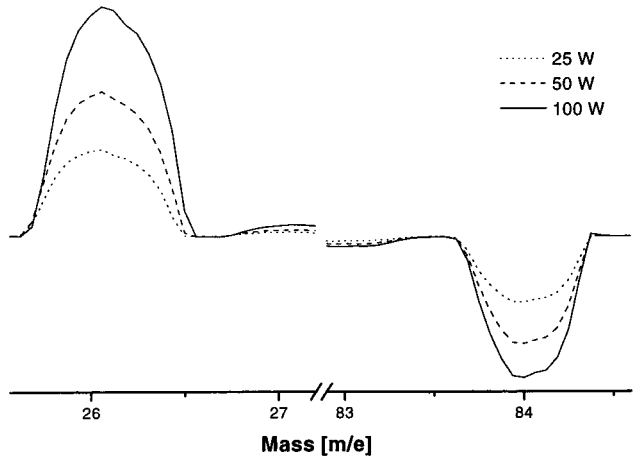

Figure 8. Characteristic netto MS peaks at different powers (at 0.06 mbar) and pressures. The netto peaks are obtained by subtracting the mass spectrum of a thiophene flow without plasma generation from the MS spectrum of a thiophene flow with plasma generation.

The assignment of the peaks is summarized in Table 2. In the mass spectrum of a thiophene flow (without plasma generation) the most prominent peaks appear at *m/e* 39, 45, 58, and 84. The peak at *m/e* 84 can readily be assigned to the thiophene monomer. The other peaks are due to fragmentation of the thiophene molecules, which takes place in the spectrometer itself. When a plasma is generated, these peaks decrease in intensity and new peaks appear in the MS spectrum, again showing that fragmentation is taking place. In Figure 8 the effect of power on the decrease and increase of peaks due to plasma generation is visualized. More fragmentation occurs with

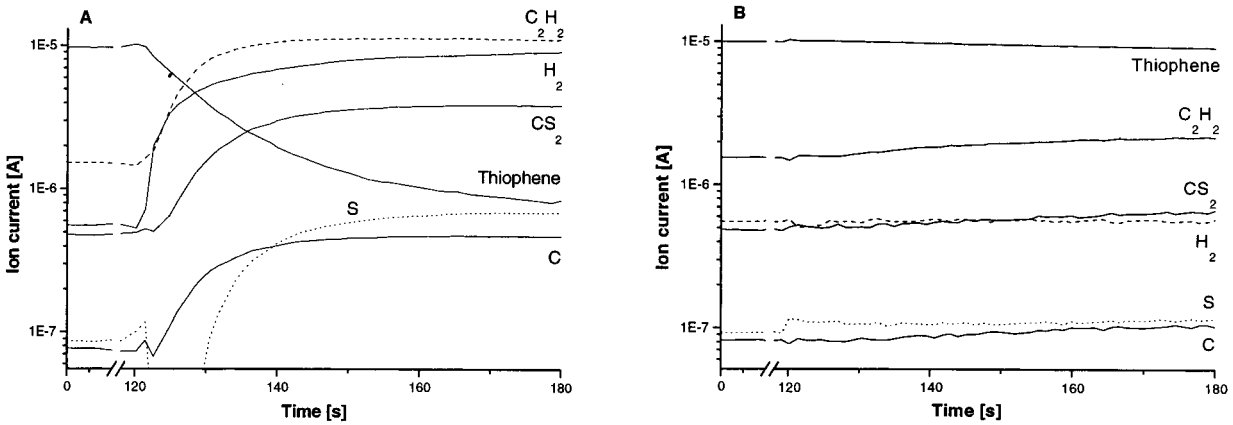

Figure 9. Intensity of the most prominent peaks in the MS spectrum as a function of time. A plasma (CW, 100 W) is generated at $t = 120$ s at a starting pressure of 0.06 mbar (A) and 0.3 mbar (B), respectively.

increasing power input, which correlates well with the OES results. The development of the most prominent peaks in the MS spectra in time is depicted in Figure 9 for two different starting pressures. At low starting pressure, the decrease of the thiophene peak and the increase of new peaks is much larger and faster than at high starting pressure. Furthermore, the peak corresponding to sulfur increases only after an "induction time". It might be possible that sulfur is only formed at a higher degree of fragmentation.

By definition, the ion current of a peak in a mass spectrum is related to the concentration of the species correlating with this peak via

$$I_i = p_{ms} c_i S_i \qquad (4)$$

with I_i = the ion current of component i [A], p_{ms} = the pressure in the mass spectrometer [mbar], c_i = the concentration of component i [−], and S_i = the sensitivity factor for i [A/mbar].

As the pressure in the MS was kept constant, the course of the ion current intensity of a peak can be taken as a measure for the course of the concentration of the component correlating with this peak. For most species, absolute concentrations cannot be calculated because the sensitivity factors are not known. However, for thiophene the sensitivity factor can be calculated from the ion current of a thiophene flow without plasma generation, assuming that the thiophene concentration is 100%. In Figure 10 the thiophene concentration is followed during plasma generation at two different starting pressures. It shows that at high pressure, deposition takes places in an environment consisting of almost pure thiophene, whereas at low pressure the environment contains much less thiophene (and much more fragments; see also Figure 9).

Characterization of PPT Layers. In Figure 2B a detail of the samples used for the conductivity measurements is shown. The electrodes are covered by the PPT layer, whereas the extensions of the electrodes are not. A good contact between the electrode extensions and the measurement leads is thus ensured. The conductivities of the iodine-doped PPT layers, summarized in Table 3, are much lower than the conductivity of polythiophene. This is most probably caused by the loss of conjugation due to the fragmentation of the monomer by the plasma polymerization process. As shown earlier, high pressures, short pulse times, high flow rates, and low power inputs result in a low amount and degree of fragmentation. Considering the fact that deposition is only taking place when a plasma is generated (see Figure 4), the influence of the deposition parameters on the fragmentation in the plasma phase was expected to be visible in the conductivity of the resulting PPT layers. Surprisingly, a Student's t-test revealed that only pressure has a significant effect ($P = 0.0013$) on the conductivity. To investigate the origin of this result, the chemical structure and composition of the PPT layers were determined with FTIR and XPS, respectively.

In Figure 11 the FTIR spectrum of a PPT layer is compared with the spectrum of T_3. The peak assignment is summarized in Table 4. Several similarities between the structure of T_3 and the PPT layer can be observed. For instance, the peaks around 3100 cm^{-1} show that the

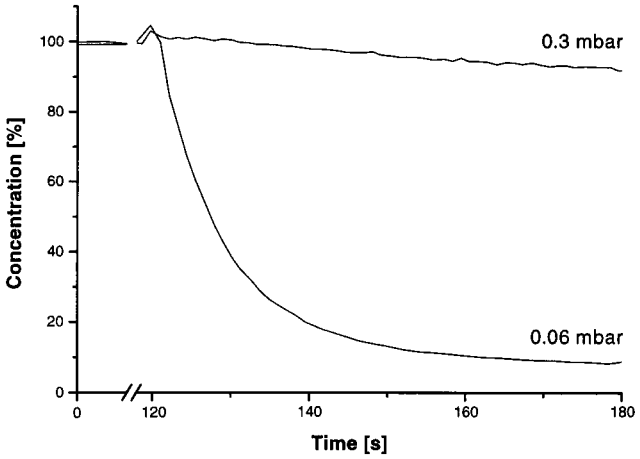

Figure 10. Concentration of thiophene (calculated from the ion current measured with MS) in the flow through the reactor as a function of time at two different starting pressures. A plasma (CW, 100 W) is generated at $t = 120$ s.

Table 3. Logarithm of the Volume Conductivities (S/cm) of PPT Layers Deposited under Different Conditions after Doping in Iodine Vapor for 5 min[a]

initial pressure (mbar)	power (W)	pulse time (t_{on}) (s)	duty cycle ($t_{on}/(t_{on} + t_{off})$)	log σ_{vol} (after doping) (log S/cm)
0.3	100	10	0.5	-5.3 ± 0.18
0.06	100	10	0.5	-7.5 ± 0.65
0.3	50	0.1	0.03	-5.6 ± 0.46
0.3	100	0.1	0.5	-5.3 ± 0.21
0.3	100	0.1	0.03	-6.2 ± 0.57

[a] The values are averaged over positions 2−4 in the reactor using two samples per position ($n = 6 \pm$ SD). No significant trend (Student's t-test, $P < 0.05$) with respect to position in the reactor was observed.

Table 4. Peak Assignment of Peaks Appearing in the FTIR Spectra (see Figure 11) of PTT Layers and 2,2′,5′,2″-Terthiophene (T_3)[14,23,57−62]

peak position (cm^{-1})		
T_3	PPT	assignment
671	664	C−S
695	706	C−H, out of plane vibration, thiophene
795	784	C−H, ring vibration
834	849	C−H, out of plane deformation, thiophene
1053		C−H, in plane deformation, thiophene
1421	1428	C−C aliphatic or ring stretching
1594	1582	C═C
	2832, 2910, 2972	CH_2 aliphatic
3041, 3072, 3103	3034, 3072, 3099	C═C−**H** stretch, thiophene
	3288	C≡C−**H**

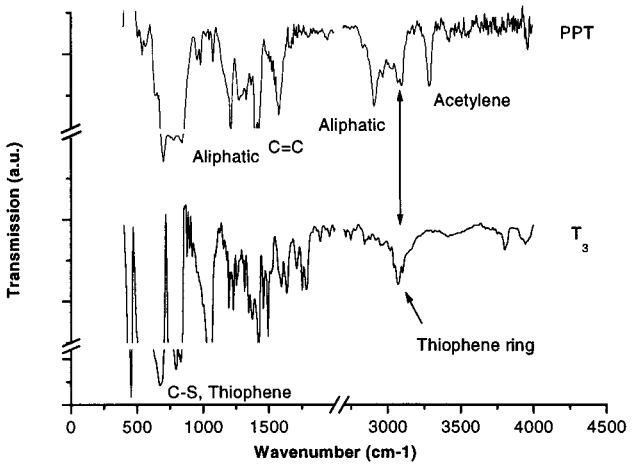

Figure 11. FTIR spectra of a PPT layer (top, 0.3 mbar, 50 W, 10 s on, duty cycle 0.5) and 2,2′,5′,2″-terthiophene (T_3) (bottom, KBr pellet).

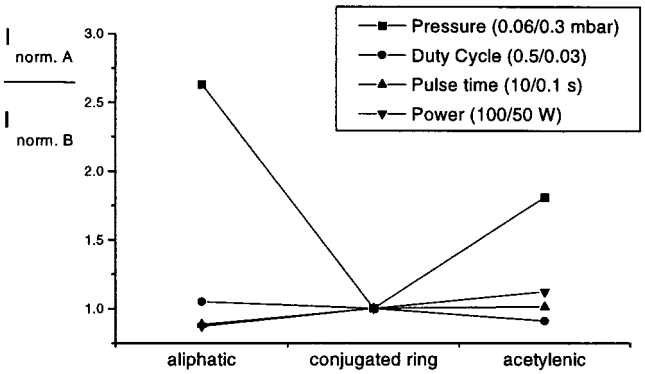

Figure 12. Intensity of peaks characteristic for aliphatic (2910 cm^{-1}), conjugated ring (3099 cm^{-1}), and acetylenic structures (3288 cm^{-1}) in the FTIR spectrum of a PPT layer deposited under condition A of a parameter (e.g. power) (normalized to the intensity of the peak at 3099 cm^{-1} in the spectrum) relative to the intensity of the same peaks in the FTIR spectrum of a PPT layer deposited under a different condition (B) for that parameter (again normalized to the peak at 3099 cm^{-1} in that spectrum).

monomer structure is partly preserved in the PPT layer. However, some terminal acetylene (3288 cm^{-1}) and aliphatic (2910 cm^{-1}) structures are also present, indicating that fragmentation has also occurred. Comparable spectra were obtained by Giungato et al. for argon-initiated PPT layers.[25]

The intensities of the peaks at 3288, 3099, and 2910 cm^{-1} were used to clarify the influence of a specific deposition parameter on the structure of the resulting PPT layer. The intensities of the peaks at 3288 and 2910 cm^{-1} in the spectrum of a PPT layer deposited at a certain value (*A*) of a parameter were normalized to the intensity of the conjugated ring peak (3099 cm^{-1}) in the same spectrum. These normalized intensities were compared with the intensities of the same peaks in the spectrum of a PPT layer deposited at a different value (*B*) of the parameter (again normalized to the intensity of the conjugated ring peak in that spectrum). The normalized intensity ratios are shown in Figure 12 for all parameters. If the PPT layer only differs in thickness and the chemical structure is the same, the normalized intensity ratio will be 1 for all three peaks.[42] Figure 12 shows that this is more or less the case for duty cycle, pulse time, and power in the ranges used. It also shows that a decrease in pressure results in a decrease of the conjugated ring structures relative to the aliphatic and terminal acetylene structures. This all correlates well with the conductivity results. It can therefore be concluded that, in accordance with the hypothesis stated earlier, the conductivity of a PPT layer increases with increasing preservation of the conjugated structure of the monomer. The most important parameter to control this is pressure (and, inherently, flow rate).

The chemical composition at the surface of the PPT layers was determined with XPS. The ratio of the atom percent of carbon over the atom percent of a characteristic atom of the monomer (i.e. C/S ratio for a PPT layer) is often used as an indication for the preservation of the monomer in the deposited layer.[24,31,33,43−54] In our case, a C/S ratio close to that of the monomer (C/S = 4) would indicate that the monomer is incorporated in the polymer without much damage. A correspondingly high conductiv-

(42) Fadini, A.; Schnepel, F.-M. In *Vibrational Spectroscopy*; Fadini, A., Schnepel, F. M., Wibbelman, C., Masson, M., Ed.; Ellis Horwood Ltd: Chichester, 1989.

(43) Gengenbach, T. R.; Griesser, H. J. *J. Polym. Sci., Part A.: Polym. Chem.* **1998**, *36*, 985−1000.

(44) Inagaki, N.; Tasaka, S.; Ishii, K. *J. Appl. Polym. Sci.* **1993**, *48*, 1433−1440.

(45) Daw, R.; Al, S.; Beck, A. J.; Brook, I. M.; Short, R. D. *Polym. Prepr.* **1997**, *38*, 1012−1013.

(46) O'Toole, L.; Short, R. D. *J. Chem. Soc., Faraday Trans.* **1997**, *93*, 1141−1145.

(47) Lopèz, G. P.; Ratner, B. D. *J. Polym. Sci. Part A: Polym. Chem.* **1992**, *30*, 2415−2425.

(48) Tanaka, K.; Nishio, S.; Matsuura, Y.; Yamabe, T. *J. Appl. Phys.* **1993**, *73*, 5017−5022.

(49) Xie, X.; Thiele, J. U.; Steiner, R.; Oelhafen, P. *Synth. Met.* **1994**, *63*, 221−224.

(50) Grünwald, H.; Munro, H. S.; Wilhelm, T. *Mater. Sci. Eng.* **1991**, *A 139*, 356−358.

(51) Munro, H. S.; Grünwald, H. *J. Polym. Sci. Polym. Chem. Ed.* **1985**, *23*, 479−488.

(52) Bhuiyan, A. H.; Bhoraskar, S. V. *Thin Solid Films* **1993**, *235*, 43−46.

(53) Gong, X.; Dai, L.; Mau, A. W. H.; Griesser, H. J. *J. Polym. Sci., Part A: Polym. Chem.* **1998**, *36*, 633−643.

(54) Tanaka, K.; Yamabe, T.; Takeuchi, T.; Yoshizawa, K.; Nishio, S. *J. Appl. Phys.* **1991**, *70*, 5653−5660.

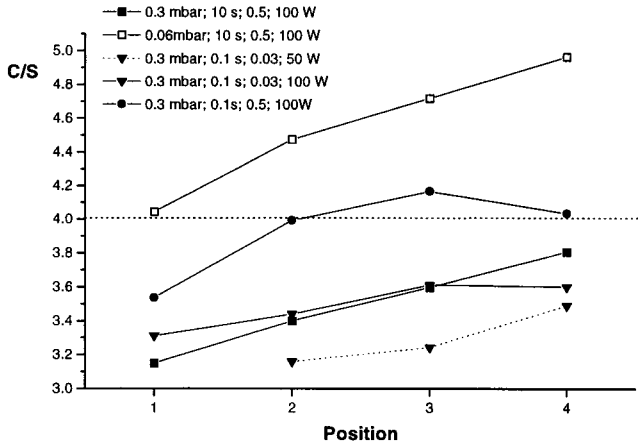

Figure 13. C/S ratio (determined with XPS) of PPT layers deposited under different conditions (pressure, pulse time, duty cycle, and power input) as a function of position in the reactor ($n = 2$, see Figure 1 for positions).

ity would be expected. The influence of the deposition conditions and the position in the reactor on the C/S ratio of the PPT layers is depicted in Figure 13. Combined with Table 3, it shows that two samples with the same C/S ratio can show a marked difference in conductivity (cf. position 1 at low pressure and position 4 at high pressure, both at 100 W; 10 s "on"; duty cycle 0.5). Furthermore, it appears that deposition at high pressure generally results in PPT layers with a C/S ratio lower than the theoretical value for polythiophene, while the conductivity of these layers was relatively high. Apparently, a C/S ratio of 4 at the surface is not a useful indicator for the conductivity of the PPT layers.

Most PPT layers deposited at high pressure have a C/S ratio smaller than 4. This means that at high pressure the formed species containing relatively more sulfur have a higher tendency for deposition than species containing relatively more carbon. However, at low pressure the C/S ratio is higher than 4. Apparently, the species containing relatively more sulfur formed at low pressure have a lower tendency to deposit than species containing relatively more carbon. This implies that the nature of the species formed at different pressures is different. From the FTIR, MS, and OES results it can be concluded that at low pressure the degree of fragmentation is higher than at high pressure. The OES results showed that more CS species are formed at low pressure than at high pressure. Although the MS spectra do not show a CS peak, the appearance of the CS_2^+ peak indicates that at least some of the species containing relatively more sulfur do not deposit. The induction time of the S^+ peak (Figure 9) shows that sulfur is formed at a later stage of the fragmentation process, i.e., when the degree of fragmentation is higher. Furthermore, at low pressure the already deposited PPT layer is more severely attacked by the plasma species. Due to the relatively labile C−S bond, more sulfur is probably liberated at low pressure than at high pressure. From these results it can be concluded that deposition under conditions that induce a higher degree of fragmentation results in PPT layers with a higher C/S ratio compared with PPT layers deposited under less fragmenting conditions.

The effect of the degree of fragmentation is also visible in the increase in C/S ratio with increasing distance from the monomer inlet. Species that deposit far away from the monomer inlet have been subjected to the plasma for a longer period of time. The degree of fragmentation is therefore higher with a correspondingly higher C/S ratio.

The effect of power on the C/S ratio is explained by the increase in electron density with increasing power input. At higher power input more electrons with sufficient energy to break the labile C−S bond attack the deposited layer. More sulfur will be liberated and a higher C/S ratio is obtained. Furthermore, the increase in electron density results in an increase in the number of collisions between electrons and other plasma species. As each collision may cause fragmentation, the degree of fragmentation will also increase, with a corresponding increase in C/S ratio.

Using longer pulse times results in a plasma resembling a continuous wave (CW) plasma. As mentioned earlier, layers deposited by a pulsed plasma show a better retention of the monomer structure than layers resulting from a CW plasma.[29,30,37] However, in our case a shorter pulse time at the same duty cycle results in a higher C/S ratio (i.e. higher degree of fragmentation). Apparently, the degree of fragmentation is more dependent on the "off" time then on the "on" time. This can be explained by the relation between the "off" time and the replenishing of the reactor with new monomer. The residence time (τ = volume/flow) of the monomer at 0.3 mbar in our system was around 1 s. Assuming the reactor is ideally stirred with a normal distribution of the residence time, after $t = 3\tau$, 99.9% of the total volume of the reactor will be replenished with monomer.[55,56] This means that when the off period is $> 3\tau$, all gas phase fragments resulting from the plasma generation will have been removed from the reactor. The plasma is then always generated in a pure monomer environment. If the off period is $<3\tau$, the plasma is generated in an environment already containing fragments. This results in a higher degree of fragmentation with a correspondingly higher C/S ratio. The higher C/S ratios found for the higher duty cycles (i.e. shorter "off" times) confirm this explanation.

Transparency. With ellipsometry it is also possible to determine the transparency of a layer irrespective of the underlying substrate. Ellipsometric measurements were carried out on both nondoped and iodine-doped (5 min) PPT layers deposited on a silicon wafer. The obtained data could be fitted with a so-called three-layer model: the ambient air, a thin PPT layer, and the substrate, taking the native silicon oxide layer on the silicon wafer into account. For the doped samples the use of an additional thin layer (i.e. diffusion front) did not lead to a significant improvement of the fit. The optical properties of the PPT layer were modeled with a Lorentzian absorption profile. The parameters, i.e., the PPT layer thickness and the characteristic parameters for the Lorentzian profile were optimized in a nonlinear fit. The effective optical thickness was calculated and the transparency was calculated using eq 3. As an example, the transparency of a 30 nm thick PPT layer is shown in Figure 14. A very high transparency (>95%) is obtained over the whole visible range. When

(55) Westerterp, K. R.; Swaaij, W. P. M. v.; Beenackers, A. A. C. M.; Kramers, H. *Residence time distribution and mixing in continuous flow reactors*, 2nd ed.; John Wiley & Sons: Chichester, 1984.
(56) Lide, D. R. *The Handbook of Chemistry and Physics*; 77th ed.; CRC Press: Boca Raton, 1996−1997.
(57) Agosti, E.; Zerbi, G. *Synth. Met.* **1996**, *79*, 107−113.
(58) Kobayashi, M.; Chen, J.; Chung, T. C.; Moraes, F.; Heeger, A. J.; Wudl, F. *Synth. Met.* **1984**, *9*, 77−86.
(59) Matsuura, Y.; Oshima, Y.; Misaki, Y.; Fujiwara, H.; Tanaka, K.; Yamabe, T.; Hotta, S. *Synth. Met.* **1996**, *82*, 155−158.
(60) Bernède, J. C.; Trégouet, Y.; Gourmelon, E.; Martinez, F.; Neculqueo, G. *Polym. Degr. Stab.* **1997**, *55*, 55−64.
(61) Ryan, M. E.; Hynes, A. M.; Wheale, S. H.; Badyal, J. P. S.; Hardacre, C.; Ormerod, R. M. *Chem. Mater.* **1996**, *8*, 916−921.
(62) Kruse, A.; Schlett, V.; Baalmann, A.; Hennecke, M. *Fresenius' J. Anal. Chem.* **1993**, *346*, 284−289.

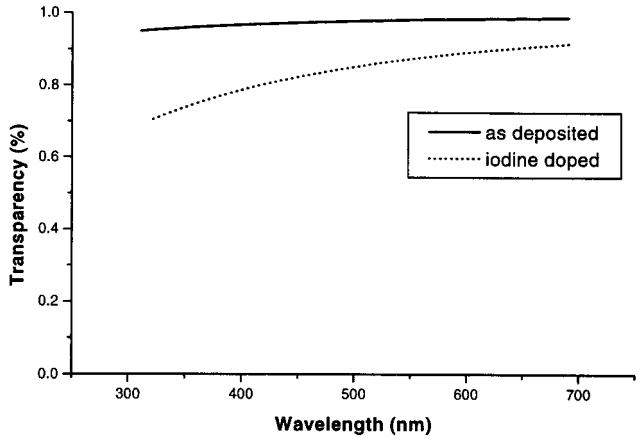

Figure 14. Transparency (calculated using eq 3) of an undoped (solid line) and doped (5 min iodine vapor, dotted line) PPT layer (30 nm) deposited at 0.3 mbar (100 W, 10 s on, duty cycle 0.5) as a function of wavelength.

doped for 5 min in iodine vapor, the transparency decreases considerably, but is still >80%. This is probably due to absorption by the iodine taken up during the doping process. The surface conductivity of such a layer was calculated to be around 1.5×10^{-11} S, which is in the range of antistatic applications.

Conclusions

Highly transparent layers with conductivities in the range of antistatic applications have been obtained by plasma polymerization of thiophene and doping with iodine. From the investigated deposition parameters, only pressure had a significant effect on the conductivity of the PPT layers. This could be related to the amount of preserved thiophene structures in the deposited PPT layer. At higher pressure more thiophene structures are built in, resulting in a higher conductivity. Opposite to what is generally accepted, a C/S ratio close to that of the starting monomer does not give conclusive information about the preservation of the monomer structure in the deposited layer. A pulsed plasma as a means to decrease the degree of fragmentation is most effective when the reactor is replenished with new monomer during the "off" time. Due to fragmentation that always takes place, plasma polymerization does not seem to be an appropriate technique to obtain conductive layers for applications requiring high conductivities.

LA000111B